Nanoscale

RSC Publishing

PAPER

Real-time optical diagnostics of graphene growth induced by pulsed chemical vapor deposition†

Cite this: *Nanoscale*, 2013, **5**, 6507

Alexander A. Puretzky,*[a] David B. Geohegan,[b] Sreekanth Pannala,[b] Christopher M. Rouleau,[b] Murari Regmi,[b] Norbert Thonnard[b] and Gyula Eres[b]

Received 22nd March 2013
Accepted 27th May 2013

DOI: 10.1039/c3nr01436c

www.rsc.org/nanoscale

The kinetics and mechanisms of graphene growth on Ni films at 720–880 °C have been measured using fast pulses of acetylene and real-time optical diagnostics. *In situ* UV-Raman spectroscopy was used to unambiguously detect isothermal graphene growth at high temperatures, measure the growth kinetics with ~1 s temporal resolution, and estimate the fractional precipitation upon cooldown. Optical reflectivity and videography provided much faster temporal resolution. Both the growth kinetics and the fractional isothermal precipitation were found to be governed by the C_2H_2 partial pressure in the CVD pulse for a given film thickness and temperature, with up to ~94% of graphene growth occurring isothermally within 1 second at 800 °C at high partial pressures. At lower partial pressures, isothermal graphene growth is shown to continue 10 seconds *after* the gas pulse. These flux-dependent growth kinetics are described in the context of a dissolution/precipitation model, where carbon rapidly dissolves into the Ni film and later precipitates driven by gradients in the chemical potential. The combination of pulsed-CVD and real-time optical diagnostics opens new opportunities to understand and control the fast, sub-second growth of graphene on various substrates at high temperatures.

Introduction

The unique thermal, electrical, and optical properties of graphene[1] may enable many potential applications involving this material, especially in the area of nanoelectronics.[2] These applications require reliable methods for the rapid synthesis of well-defined crystalline patches of graphene, and in many cases, at specific locations on different substrates. Among the many different methods of graphene synthesis, chemical vapor deposition (CVD) is the most attractive since it permits the growth of graphene on metal catalyst-patterned substrates.[3]

CVD of graphene includes the processes of decomposition of hydrocarbon gas on metal catalyst foils or films, followed by the self-assembly of carbon into graphene. Among the many different metals employed for graphene growth, Cu[4–12] and Ni[13–20] are the most widely used and studied. Most of the progress toward optimizing the growth of graphene in (i) large single-crystals with (ii) controlled numbers of layers over (iii) large surface areas has resulted from the empirical variation of the CVD growth parameters (temperature, partial pressures and flows of the feedstock and buffer gases, *etc.*).[5,8–12,21] Despite such progress, it has been difficult to achieve a fundamental understanding of the growth mechanisms. In many of these experiments, it is commonly accepted that graphene grows by segregation of surface carbon in the case of metals with low carbon affinity such as Cu, and by a dissolution/precipitation mechanism in the case of metals with high carbon affinity, such as Ni, whereby carbon atoms first dissolve in the metal at high temperatures and then precipitate to its surface upon cooling to form graphene. While in conventional CVD experiments it takes minutes to grow graphene on Cu,[22,23] and similar growth times have been reported on Ni[13,15,17,18] substrates, graphene growth on metals with high carbon affinity should be very similar to the first stage of SWNT growth – *i.e.*, the nucleation of a nanotube cap – which clearly can occur very rapidly at the growth temperature.[24–26] Very rapid, sub-second growth of graphene on Ni foils has been demonstrated in laser direct-write processing.[27]

To clarify the mechanisms and kinetics of graphene growth, several key *in situ* diagnostic experiments have been performed, although under the well-controlled conditions conducive for surface science measurements.[22,28,29] For example, *in situ* low-energy electron microscopy was used during deposition of elemental carbon on Cu to confirm that graphene grows by segregation of surface carbon at the edges of lobed structures at high temperatures.[22] In the case of Ni, however, CVD growth of

[a]*Oak Ridge National Laboratory, Oak Ridge, TN, USA. E-mail: puretzkya@ornl.gov; Fax: +1-865-576-7462; Tel: +1-865-241-9482*

[b]*Oak Ridge National Laboratory, Oak Ridge, TN, USA*

† Electronic supplementary information (ESI) available: A movie of graphene growth after exposure to a single C_2H_2 pulse, modeling of gas dynamics, Raman map and spectra of graphene transferred to a SiO_2/Si substrate, time-resolved reflectivity upon exposure to a pure Ar pulse, Raman map of I(2D)/I(G) ratios for 800 °C and 20% C_2H_2 concentration, comparison of Raman spectra of a single layer suspended graphene at 532 nm and 404.5 nm, processing of reflectivity curves for comparison with growth kinetics based on Raman measurements. See DOI: 10.1039/c3nr01436c

graphene by both surface assembly and dissolution/precipitation mechanisms have been observed by a variety of *in situ* diagnostic, during cooling, and even sometimes at the growth temperature. For example, with very low pressures of propylene (C_3H_6) gas on Ni (111), real-time photoemission spectroscopy indicated self-limited surface-growth of graphene from adsorbed C_3H_6 fragments at the growth temperature, without any significant change in the photoemission spectra upon cooling.[29] On the other hand, *in situ* X-ray photoelectron spectroscopy (XPS) and *in situ* X-ray diffraction (XRD)[30] studies both concluded that CVD graphene grows on Ni by dissolution/precipitation. However, in contrast to the commonly accepted precipitation mechanism proposed during cooling,[13,16] graphene appears to grow on Ni films through isothermal diffusion of the subsurface dissolved carbon and does not require cooling. Finally, *in situ* spectroscopic ellipsometry of carbon deposition on Ni films during CVD was correlated to the number of graphene layers that formed to yield some insight into its growth kinetics, indicating that graphene forms both at growth temperature and during cooling.[31] These *in situ* experiments indicate that, similar to carbon nanotubes,[32–36] graphene can grow by more than one mechanism depending on the conditions,[29,30,37] and that easily-implemented, real-time diagnostics are necessary to understand and optimize the kinetics and quality of graphene grown under conventional CVD growth conditions.

Here we present UV-Raman spectroscopy, optical reflectivity, and microscope-based videography as implementable real-time diagnostics to measure the kinetics of graphene nucleation and growth at high temperature, and to unambiguously determine the fraction of graphene that precipitates upon cooldown. Sub-second pulses of gas with varying acetylene partial pressure are employed to understand graphene nucleation and growth kinetics resulting from well-defined doses and exposures, allowing the exploration of different growth stages. Both the growth kinetics and the fractional isothermal precipitation are shown to be governed by the C_2H_2 partial pressure in the CVD pulse for a given film thickness and temperature. High partial pressures are shown to drive up to 94% of the graphene growth to occur within the ~1 s gas pulse period, while lower partial pressures initiate isothermal growth that continues seconds after the gas pulse. The observed flux-dependence of the isothermal growth is discussed in the context of a dissolution precipitation model.

Experimental

Pulsed CVD of graphene

The pulsed CVD reactor was based on a high temperature microscope stage (Linkam, TS 1500) (Fig. 1a) which was modified by replacing all of the electrical feedthroughs with O-ring sealed versions to allow operation at gas pressures down to 10^{-3} Torr. For pulsed growth, Ar (100 sccm) and H_2 (20 sccm) gases were flowed continuously through the reactor, and acetylene gas was injected from a pulsed valve (Parker model: 099-0340-900) using a 1.0 ms wide electrical pulse supplied by a digital delay generator (Stanford Research Systems, DG545), which was subsequently amplified to drive the valve. The amount of gas introduced per pulse depends on the backing pressure supplied

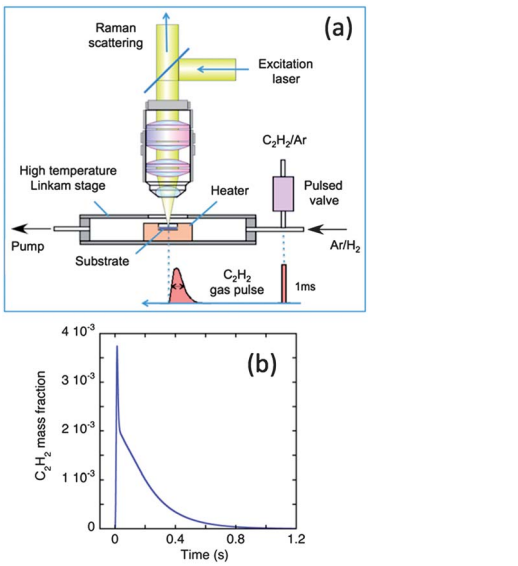

Fig. 1 (a) Schematic of the experimental setup used for *in situ* Raman measurements of graphene growth by pulsed CVD. (b) Calculated C_2H_2 gas pulse at the center of a Ni/SiO_2/Si substrate.

to the pulsed valve and was 0.2 standard cubic centimeters (scc) at 20 psi (1773 Torr), as determined from pressure rises measured in a calibrated volume. With a backing pressure of 400 Torr and a 4 : 1 Ar : C_2H_2 mixture (C_2H_2 concentration = 20% or the maximum used in these experiments) the amount of acetylene injected in a gas pulse was therefore 0.009 scc. To compare the conditions during a 0.2 s (FWHM) gas pulse (Fig. 1b) to those used in continuous CVD flow reactors, the equivalent flow rate of acetylene and its partial pressure for the richest (20% C_2H_2) gas mixture were estimated to be ~2.7 sccm and ~0.14 Torr, respectively. All experiments were carried out at a total pressure of ~7 Torr, and in the temperature range of 720–880 °C with heating and cooling rates of 60 °C min^{-1}.

To understand the gas propagation dynamics, including the shape and the temporal width of the C_2H_2 pulse at the substrate location, 3D modeling of the CVD reactor was performed (see ESI,† Section 1). Fig. 1b shows the C_2H_2 mass-fraction at the center of the substrate as a function of time after opening the valve. According to this calculation the C_2H_2 gas pulse has a narrow initial peak (~20 ms FWHM) followed by a long tail (~200 ms FWHM with a duration of ~1 s), which can be explained by relatively long (up to 1 s) trapping of acetylene in the stage due to formation of vortices in the gas flow. The C_2H_2 peak arrives at the center of the substrate 14 ms after actuating the valve. A more detailed description of this model, which includes the 3D distribution of the gas flow velocity, temperature, and mass fraction of acetylene in the stage, is given in the ESI.† These calculations show that the shape and duration of the feedstock gas pulse will allow one to study fast nucleation and growth kinetics occurring within sub-second times.

Pulsed gas introduction therefore provides precise control of the amount of carbon released for CVD of graphene on the surface of the Ni films. In this study only a single gas pulse of Ar/C_2H_2 was used, and regardless of the partial pressure of C_2H_2

used in the experiments, the total pressure used to back the pulsed valve was maintained at 400 Torr to ensure constant gas dynamics.

Sample preparation

A 0.5 μm Ni film was deposited onto a 5 mm × 5 mm Si substrate with a 0.5 μm SiO_2 buffer layer using electron beam evaporation. All catalyst substrates were pre-annealed in a furnace at 800 °C for 15 minutes in flowing Ar (2000 sccm)/H_2 (200 sccm) at atmospheric pressure to develop a grain structure. This time was found sufficient to minimize further grain development upon heating to the growth temperature in the microscope stage as monitored by *in situ* optical reflectivity and microscopy. This substrate was placed inside a ceramic boat on a thin sapphire disk in the heater assembly of the microscope stage (Fig. 1a).

Temperature measurements

The microscope stage thermocouple readings were calibrated to determine the actual surface temperature of the Ni/SiO_2/Si samples using the known shifts and linewidths (FWHM) of the 520 cm^{-1} Si line in the Stokes and anti-Stokes regions of the Raman spectrum of the SiO_2/Si substrate.[38,39] This method is more reliable than that based on the integrated intensity ratio of the Stokes and anti-Stokes Raman lines, since the ratio method requires correction factors for the absorption coefficients and the Raman cross sections at the excitation, Stokes, and anti-Stokes frequencies, which are not well known.

In situ Raman measurements

Raman spectra were acquired using a single spectrometer stage of a confocal, tunable micro/macro-Raman system (Jobin Yvon Horiba, T64000) equipped with a liquid nitrogen cooled CCD detector (Symphony Horiba JY). A continuous wave (cw) wavelength-stabilized diode laser (404.5 nm, 35 mW, Ondax, 2.6 mW at the sample) was used as a UV-excitation source for Raman spectra acquisition where blackbody radiation background at elevated temperatures could be minimized. To filter out the excitation laser light, a 405 nm edge filter (Semrock) was used. To suppress the amplified spontaneous emission from the laser a reflective volume holographic grating beam splitter (Ondax) was used. The laser beam on the sample was defocused to a spot size of ~24 μm to sample growth over many Ni grains, and to minimize heating or damage of the graphene in these experiments.

The scattered light was collected through a microscope in the back-scattering configuration using a long working distance microscope objective (50×, NA = 0.5). To monitor both the G- and 2D-graphene bands simultaneously, a low dispersion grating (900 grooves per mm) was used in the spectrometer.

To perform kinetics measurements the CCD detector acquired spectra in 1 second acquisitions. The pulsed gas valve was fired 0.8 ms after a synchronization pulse output was received from the shutter on the CCD detector that signaled the first acquisition period in a sequence. The valve opening was detected by a microphone attached to the valve, and the relative timing was adjusted with a digital delay generator (SRS DG545).

In situ videography and time-resolved reflectivity

The same modified (Linkam) microscope stage was used with a different microscope (Olympus BH-2) equipped with an ultra-long working distance (22.5 mm) objective (50×, NA = 0.42) to conduct *in situ* microscope-based videography and time-resolved reflectivity measurements. Video movies of graphene growth were acquired through the microscope using a CCD camera with a frame rate of 30 fps. Time resolved reflectivity of the white light illumination on the substrate was simultaneously measured at 50 samples per s using a photodiode attached to one of the microscope's eyepieces and a Keithley 6485 picoammeter to record the photocurrent. A microphone attached to the valve was used to trigger a pulse from a digital delay generator (SRS DG545) which was summed with the photocurrent to leave an easily discernible time mark at a preset delay to synchronize the valve opening with the reflectivity photocurrent (see Fig. S3, ESI†). To verify the effect of further development of the Ni film grain structure on its reflectance a pre-annealed Ni film (see Sample preparation section) was heated up to 800 °C in flowing Ar/H_2 (100/20 sccm, respectively) and exposed to a single pulse of pure Ar (Fig. S3, ESI†). In this case the reflectivity signal did not show any changes upon exposure to the Ar pulse and exhibited only a small decrease (~0.5%) after 60 s annealing time at 800 °C.

Ex situ characterization

As synthesized graphene was investigated by scanning electron microscopy (Zeiss, Merlin SEM at ~3 kV). *Ex situ* Raman measurements were performed using a cw 532 nm laser (up to 10 mW at sample location).

Results and discussion

Characterization of graphene grown by pulsed CVD

Few-layer graphene with low defect density and complete coverage was grown rapidly on Ni substrates using single, sub-second pulses of diluted acetylene at high temperatures. The number of graphene layers and the surface coverage were found to depend on the growth temperature, the partial pressure of the feedstock gas, the Ni film thickness and its grain structure and size.

Fig. 2 shows SEM images of graphene grown on Ni films at two different temperatures (720 °C and 840 °C) for three

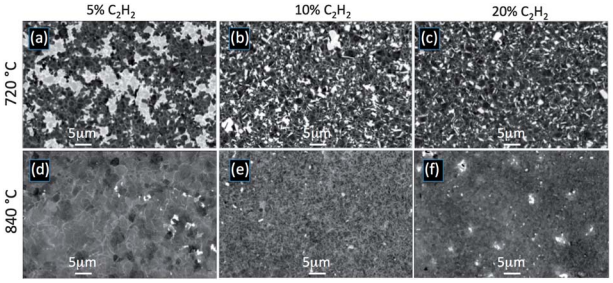

Fig. 2 SEM images of graphene grown on 0.5 μm thick Ni films using a single pulse of Ar/C_2H_2 gas for different C_2H_2 concentrations (indicated at the top of each column). The growth temperatures were (a)–(c) 720 °C and (d)–(f) 840 °C.

concentrations of C_2H_2 (5%, 10%, 20%) in the injected gas mixture (corresponding to 0.035, 0.07, and 0.14 Torr acetylene partial pressures during a ~0.2 s pulse in the reactor). At a growth temperature of 720 °C, the surface coverage is not complete and depends on the concentration of C_2H_2. For the growth at 720 °C, the surface coverage of graphene can be estimated from these SEM images as 69, 77, and 86% for C_2H_2 concentrations of 5, 10, and 20%, respectively. At the higher growth temperature of 840 °C, however, complete surface coverage was observed for all concentrations of C_2H_2 used in this study.

To characterize the quality of the graphene grown by pulsed CVD on Ni films we compared the room temperature Raman spectra with that from a reference sample of single layer, single-crystal graphene suspended over the 7 μm holes of a 2000 mesh Au TEM-microscope grid (Fig. 3) measured using the same experimental setup. The ratios of the 2D and G peak intensities, $I(2D)/I(G)$, for these two cases are very similar: 3.7 for the Ni-film and 3.2 for the suspended single layer graphene. However, the similarity in the $I(2D)/I(G)$ does not mean that graphene on the Ni film is also a monolayer since bilayer graphene can exhibit the same $I(2D)/I(G)$ ratio depending on the layer stacking.[17,19,40] Moreover, the strong interaction between a graphene monolayer and a Ni (111) surface is predicted to result in significant changes in its electronic structure,[41] which could significantly influence the intensity and frequencies of its Raman modes. One experimental study supports this prediction, reporting that the Raman spectra of monolayer graphene on Ni was not detectable in the spectral region from 1000 to 3000 cm^{-1}, while bilayer and few-layer graphene was observable.[42] The transformation of the Raman spectrum of graphene due to this strong coupling to the Ni (111) surface is not clear yet and requires further theoretical and experimental investigations.

In our case the strong Raman G- and 2D-peaks of graphene observed on Ni films (Fig. 3) with the $I(2D)/I(G)$ ratio ~3.7 can be explained by the formation of turbostratic bilayer graphene under these growth conditions. Turbostratically stacked bilayer graphene has two distinct features, which result from the decoupling of the graphene layers, *i.e.*, a narrow 2D band compared to that of the AB stacked graphene and an $I(2D)/I(G)$ ratio that exceeds that for single layer graphene.[43,44]

To estimate the width and the $I(2D)/I(G)$ ratio and also to explore the uniformity of the graphene layers across the Ni film, spatial mapping of the Raman spectrum was performed for as-grown graphene on the Ni film (Fig. 4) and after transfer to a SiO_2 (0.3 μm)/Si substrate (Fig. S4, S5, and Table S1, ESI†). Fig. 4a shows the $I(2D)/I(G)$ ratio Raman map measured for graphene grown at 840 °C using a 532 nm excitation wavelength and a 1 s acquisition time for each point. The corresponding SEM image is shown in Fig. 2d. The map demonstrates ~10 μm patches with a 2D/G ratio > 4. For example, point 5 (Fig. 4a)

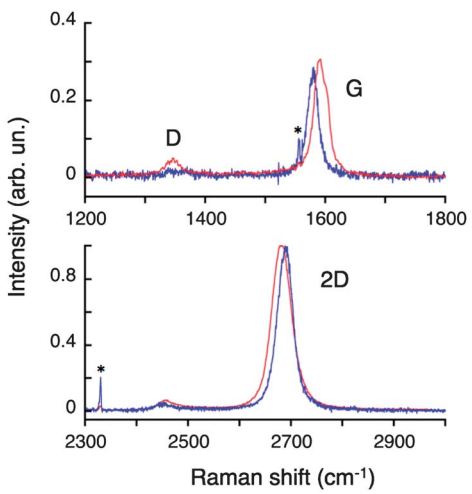

Fig. 3 Raman spectrum of graphene grown on a Ni film by pulsed CVD at 880 °C and 17% concentration of C_2H_2 (blue curves). Raman spectrum of suspended single layer, single crystal graphene grown on Cu foil by low pressure, continuous CVD and transferred to a 2000 mesh microscope grid is shown for comparison (red curves). All spectra are normalized to the intensities of the 2D-bands. The narrow peaks marked by asterisks are ambient O_2 (1556 cm^{-1}) and N_2 (2331 cm^{-1}) Raman lines.

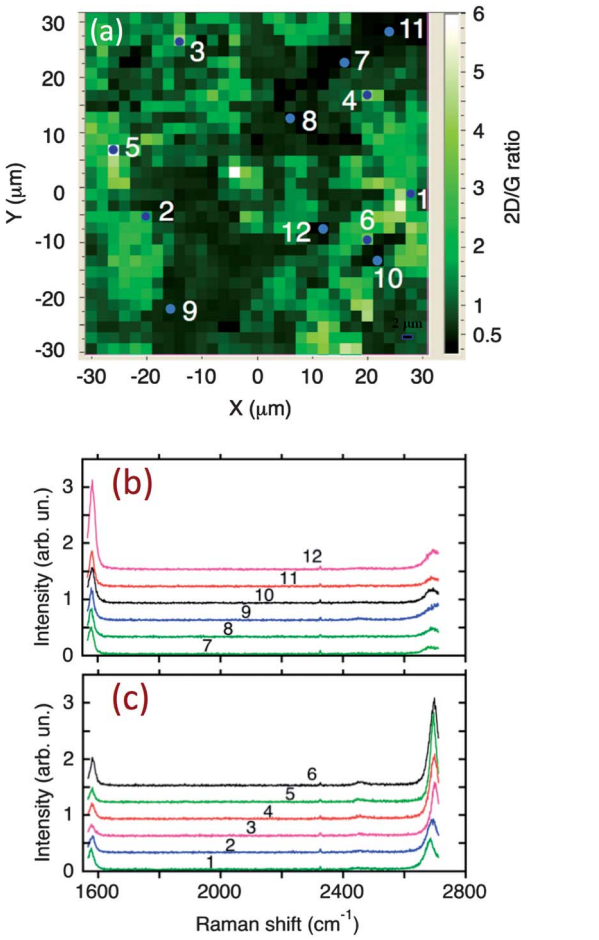

Fig. 4 (a) Raman map (62 μm × 62 μm) of the $I(2D)/I(G)$ ratios measured for graphene grown at 840 °C using a 5% concentration of C_2H_2. The average intensities of the 2D- and G-bands in the range of 2690–2701 cm^{-1} and 1574–1585 cm^{-1}, respectively, were used to calculate the ratios. The corresponding SEM image is shown in Fig. 2d. The 12 dots on the map indicate the positions for the corresponding Raman spectra shown below in (b) points 7–12 and (c) points 1–6. The map was acquired using a 532 nm excitation wavelength (laser spot size at the sample ~2 μm) with 1 s acquisition time for each point and 2 μm increments.

shows the G- and 2D-bands at 1580 cm^{-1} and 2695 cm^{-1}, respectively, with corresponding bandwidths of 18 cm^{-1} and 24 cm^{-1} (FWHM), and a $I(2D)/I(G)$ ratio of 6.7 (Fig. 4c), which can be attributed to turbostratic bilayer graphene. This graphene is intermixed with few layer graphene ($I(2D)/I(G) < 1$, Fig. 4b) having domains of approximately the same size. Transfer of graphene grown under these conditions to a SiO_2 (0.3 μm)/Si substrate using a standard transfer procedure (see Fig. S4) gives similar results in the regions composed from turbostratic bilayer graphene, but with an even higher $I(2D)/I(G)$ ratio (up to 13.5) and a similarly narrow 2D band (~24 cm^{-1}, FWHM) (see Fig. S5 and Table S1†).

Increasing the relative concentration of C_2H_2 (20%) at the same growth temperature results in growth of few layer graphene with a more uniform distribution of the number of layers across the Ni film (see Fig. S6, ESI†). The corresponding Raman map of graphene grown under these conditions and transferred to a SiO_2/Si substrate (see Fig. S7, ESI†) shows Raman spectra, which are very similar to those measured on the Ni film (Fig. S6, ESI†). This comparison confirms synthesis of few layer graphene under these growth conditions.

In situ Raman spectroscopy

Acquiring real-time Raman spectra of graphene growth at elevated temperatures was optimized in the described confocal microRaman spectroscopy setup subject to the following experimental observations: First, a 1 second spectral acquisition time was chosen to match the observed kinetics and gas pulse width, yet still provide sufficient signal-to-noise ratio. Second, 404.5 nm excitation was utilized to acquire Raman spectra where the blackbody radiation background was minimized, however at the expense of reduced 2D band intensity.[45] We measured the influence of the excitation wavelength on the 2D/G ratio by comparing Raman spectra measured at 532 nm and 404.5 nm using the same location on single layer graphene suspended over a microscope grid (see Fig. S8, ESI†). At room temperature it was found that operating at 404.5 nm reduces the $I(2D)/I(G)$ by a factor of 3.7 when compared to operating at 532 nm. Third, while the integrated intensity of the G-band remains constant for graphene on Ni films when the temperature increases from 25 °C to 840 °C, allowing its use as an *in situ* diagnostic of graphitic carbon, the integrated intensity of the 2D band was found to decrease linearly by a factor of 1.5 over the same range. Hence, we did not use the 2D band for quantitative estimates of graphene formation. Fourth, the laser spot was defocused to a relatively large 24 μm diameter on the Ni substrate to ensure that the laser was not heating or damaging graphene during or after growth. All of these factors were considered in the choice of operating conditions for the measurements.

Fig. 5 shows typical Raman spectra (measured with 1 s acquisition times) for graphene growth at 800 ± 20 °C upon exposure to a single C_2H_2 pulse initiated at time $t = 0$ (see Fig. 1b). A narrow G-band is observed at 1566 cm^{-1} during the first 1 second acquisition. The 2D-band can just be discerned, but with very low intensity. Fig. 6 plots the integrated intensity

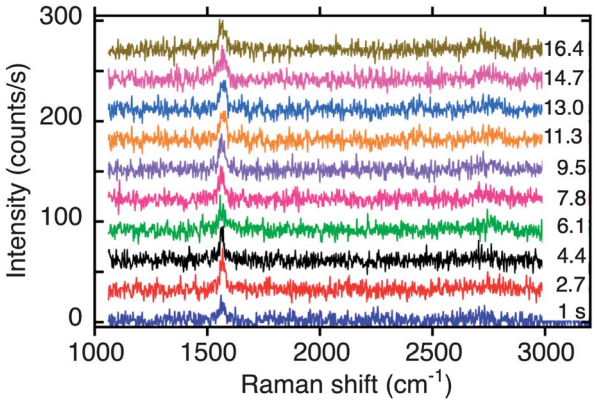

Fig. 5 (a) Time evolution of the G- and 2D-Raman bands of graphene measured *in situ* at 800 °C using an excitation wavelength of 404.5 nm with acquisition time of 1 s after exposure to a single pulse of C_2H_2 (20% concentration) at $t = 0$. The bottom spectrum corresponds to the first acquisition from $t = 0$ to $t = 1$ s. The end times for all subsequent acquisitions are indicated at the right. The corresponding spectra are offset vertically by 30 counts per s relative to each other.

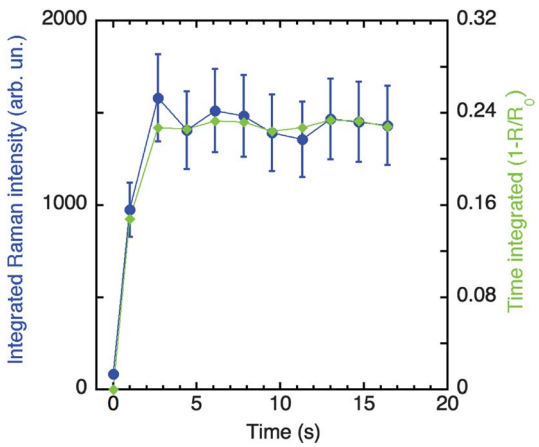

Fig. 6 Integrated Raman scattering intensity of the G-band (from 1450 to 1700 cm^{-1}) measured *in situ* during graphene growth at 800 °C (20% C_2H_2) (see Fig. 5) as a function of time after opening the pulsed valve. The points correspond to the ends of the 1 s acquisition intervals and the point at $t = 0$ shows background, *i.e.*, corresponds to the interval from –1 to 0 s. The green curve (diamonds) shows the reflectivity signal ($1 - R/R_0$) integrated over time in the corresponding Raman acquisition intervals (see Fig. S9, ESI†).

of the G band as a function of time after the valve opens. The second acquisition (from 1.7 s to 2.7 s) shows ~1.5 times higher intensity. All subsequent acquisitions do not show any changes in the integrated intensity of the G-band (Fig. 6). This means that under these particular growth conditions, isothermal graphene growth initiates during the first 1 second acquisition, and is completed by $t = 2.7$ s.

To understand if there is any additional precipitation of graphene during cooling, *in situ* Raman spectra were acquired during ramping (at 60 °C min^{-1}) back to room temperature. In this case, a 20 s acquisition time was used to increase the signal to noise ratio. Fig. 7a compares Raman spectra of graphene grown at 800 °C by a single Ar/C_2H_2 gas pulse, measured both at the growth temperature and after cooling to room temperature.

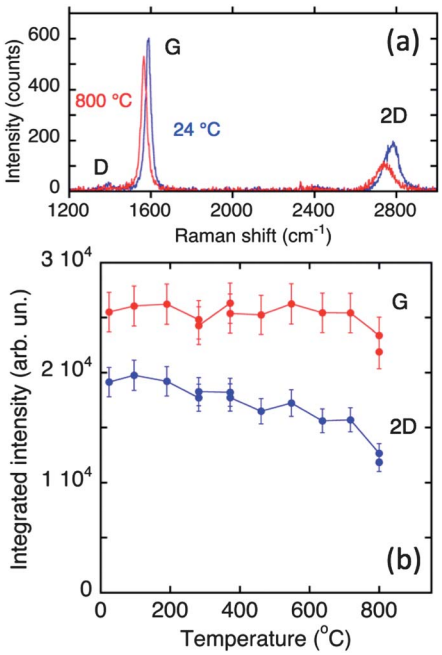

Fig. 7 (a) Raman spectra of graphene measured at the growth temperature of 800 °C (20% C_2H_2) (red) and after cooling to room temperature (blue) using an excitation wavelength of 404.5 nm and acquisition time of 20 s. (b) Integrated intensities of the G- (from 1450 to 1700 cm^{-1}) and 2D- (from 2550 to 2950 cm^{-1}) Raman bands measured during cooling from the growth temperature (800 °C) to room temperature.

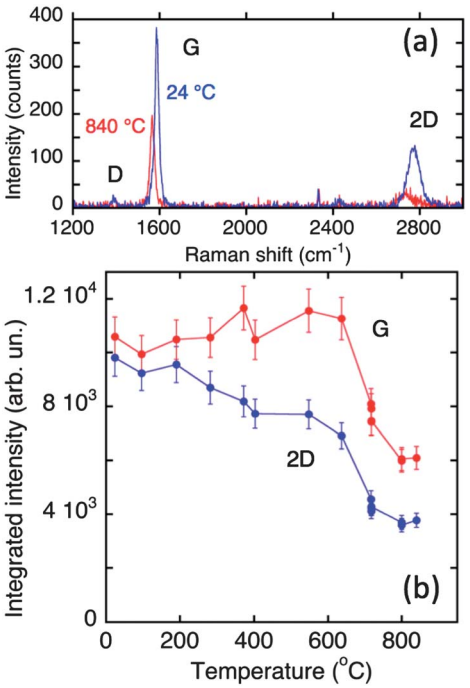

Fig. 8 (a) Raman spectra of graphene measured at the growth temperature of 840 °C (5% C_2H_2) (red) and after cooling to room temperature (blue) using an excitation wavelength of 404.5 nm and acquisition time of 20 s. (b) Integrated intensities of the G- (from 1450 to 1700 cm^{-1}) and 2D- (from 2550 to 2950 cm^{-1}) Raman bands measured during cooling from the growth temperature (840 °C) to room temperature.

At 800 °C, the G- and 2D-bands exhibit downshifts relative to their room temperature positions of 21 cm^{-1} and 44 cm^{-1}, respectively. Temperature-dependent Raman spectral lineshifts in graphene have been explained theoretically by its lattice anharmonicity and by strain induced by thermal expansion mismatch with the substrate. The linewidths of the bands are defined by the anharmonic phonon–phonon and electron–phonon interactions.[46,47] A larger increase in the integrated intensity of the 2D-band (~40%) is observed in this case. The integrated intensity of the G-band is a good measure of graphitic carbon and has been used for *in situ* monitoring of carbon nanotube growth.[48–53]

Fig. 7b shows integrated intensities of the G- and 2D-bands measured during cooling to room temperature as a function of temperature. The integrated intensity of the G-band remains constant in the temperature range from 720 °C to 25 °C, although a very small (~10%) increase is observed from 800 °C to 720 °C. Overall, this indicates that less than 10% of graphene grows during cooling for these growth conditions. In contrast to the G-band, the integrated intensity of the 2D-band increases linearly from 720 °C to 25 °C. The linear temperature dependence of the integrated 2D-band intensity was confirmed also in other runs where the G-band remained constant, so we conclude it is not related to the precipitation of graphene.

At reduced concentrations of C_2H_2 (5%), however, the measurements indicate that a higher fraction of graphene forms on cooling. Fig. 8 shows that following pulsed isothermal growth at 840 °C, the G-band increases by ~50% during cool-down between 840 and 640 °C and remains approximately constant during further cooling from 640 °C to room temperature. This means that approximately 50% of the graphene grows isothermally at 840 °C, and 50% grows during cooling.

Fig. 9 summarizes the results of 10 growth runs conducted at different temperatures and C_2H_2 concentrations. One can see that even at the same growth conditions there are some deviations in the estimated amount of graphene precipitated during

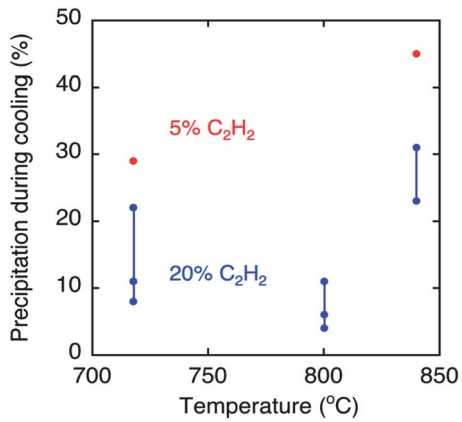

Fig. 9 Summary of the results on graphene precipitation during cooling based on *in situ* Raman measurements at different growth temperatures and C_2H_2 concentrations. Each point corresponds to a different run. The percentage of precipitation during cooling was estimated based on the temperature dependence of the integrated intensity of the G-band as described for the runs shown in Fig. 7 and 8.

cooling. This is likely due to non-uniformities in the Ni grain structure within different observation spots. The measurements also show that decreasing the C_2H_2 concentration by a factor of 4 increases the fraction of graphene that precipitates during cooling by a factor of ~2. The lowest fraction of precipitation during cooling (an average of 6%) is observed at 800 °C and high (20%) C_2H_2 concentration. Note that the actual values of the precipitated fractions could be even lower for the case where the G-band of single layer graphene does not appear in the Raman spectra of graphene grown on Ni films.

These *in situ* Raman experiments clearly show that under pulsed CVD conditions graphene grows isothermally at the growth temperature with some fraction precipitated during cooling, the amount depending on the growth temperature and C_2H_2 concentration (Fig. 9). Decreasing the C_2H_2 concentration as well as increasing the growth temperature results in a higher fraction precipitated during cooling, which in the present case can reach almost 50%. *In situ* Raman measurements also show that graphene appears fast, within 1 s after the introduction of a C_2H_2 pulse. Currently, a more precise Raman spectroscopic determination of the onset time for the appearance of graphene is limited by the signal-to-noise ratio of our Raman setup.

Real-time optical imaging and time-resolved reflectivity

To explore faster growth kinetics, direct video-rate microscopy and *in situ* white light reflectivity were used. However, these techniques are not selective to graphene, and must be verified using a graphene-selective *in situ* diagnostic such as the Raman scattering technique employed above. Another advantage of this approach is its ability to detect even a single layer graphene on metal substrates including Ni.

Fig. 10 shows six selected frames from a movie (see ESI†) taken during graphene growth using a single pulse of C_2H_2 at 800 °C. These images show that during the first 0.5 s after opening the pulsed valve, there is no visible deposition of graphene on the Ni surface. After this time, however, multiple microns-sized graphene patches develop simultaneously across the field of view and grow rapidly. Those regions with a reflectivity decrease of >5% are shaded in red in Fig. 10. After 1.3 s ~85% of the whole surface is covered with graphene patches without any changes at later times.

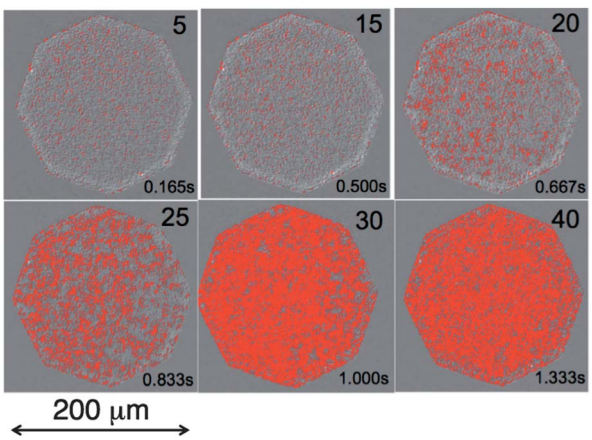

Fig. 10 A set of six selected frames from a movie taken during graphene growth using a single pulse of C_2H_2 at 800 °C (backing Ar/H_2 (5 : 1) pressure ~300 Torr). The field of view is restricted by an octagonal microscope aperture. The numbers indicate corresponding frames (top) and times (bottom) starting from valve opening, which was defined by a slight shift in the image due to the acoustic shock generated by the valve. The graphene patches were colored in red for clarity.

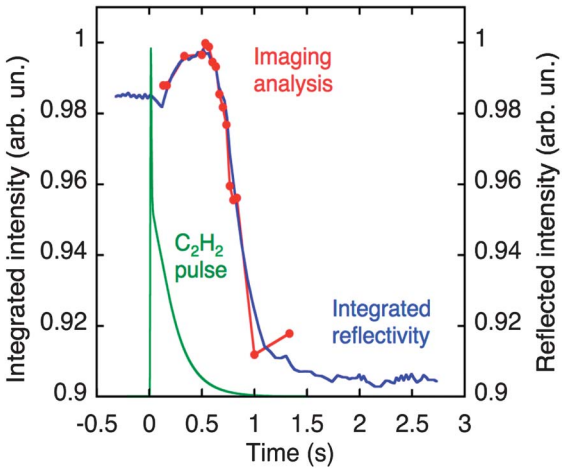

Fig. 11 Normalized intensity of the microscope white light reflected from Ni/SiO_2/Si substrate measured with a photodiode as a function of time after release of a C_2H_2 pulse (blue curve) at 800 °C. Integrated intensities of the sequential frames from a movie (Fig. 10) obtained by image analysis (dots). The calculated C_2H_2 gas pulse is shown for comparison.

Fig. 11 shows the time evolution of the reflected intensity measured by the photodiode after the release of a single pulse of C_2H_2. The integrated intensities of the images selected from the movie (see ESI† and Fig. 10) are shown on the figure as well. The trends are almost identical, and show a slight ~2% increase in the reflected intensity during the first 0.5 s after the valve opens. After this, the reflected intensity drops rapidly by ~8% at the 1 s mark, with only minor changes (<1%) thereafter. Both imaging and reflectivity data show an induction period (~0.5 s) where the reflectivity reaches its maximum, followed by a rapid decrease and saturation in reflectivity corresponding to the graphene growth period. The reason for the small initial increase in the reflected intensity is unclear, but may be due to the accumulation of carbon precursors on the surface or in the grain boundaries, or dissolution-induced change in the surface structure of the Ni grains that result in surface smoothening of the film to produce a more reflective surface.

To confirm that these reflectivity-based kinetics measurements correspond to graphene growth, we duplicated the pulsed-CVD growth conditions of the *in situ* Raman measurements presented in Fig. 5 and 6 (see Fig. S9, ESI†). The function $1 - R/R_0$ (R_0 and R are the reflected intensities before and after opening the valve, respectively) was integrated over 1 s intervals at the same times used during the Raman experiments (see Fig. 5 and 6). The resulting integrals are plotted in Fig. 6. One can see that the magnitude and temporal behavior of the reflectivity signal measured by the photodiode match the G-band intensity from the *in situ* Raman measurements obtained with lower time resolution. Optical reflectivity therefore appears

to be a useful real-time optical diagnostic for graphene growth that can be readily-implemented in various types of reactors.

Fig. 12 shows the reflectivity response during the pulsed-CVD of graphene at 800 °C for different C_2H_2 concentrations and Ni film thicknesses. In all cases there is an initial small increase in reflectivity during exposure to the C_2H_2 pulse followed by a decrease due to graphene formation. At a C_2H_2 concentration of 5% most of the growth is observed to occur long *after* the C_2H_2 has cleared from the microscope stage. As shown in Fig. 12a, increasing the acetylene concentration drives faster isothermal graphene growth. At 20% C_2H_2 concentration, the growth time is <1 second. Decreasing the Ni film thickness also results in a reduction in growth time (Fig. 12b).

The induction and growth times for the 0.5 μm thick film from Fig. 12a are plotted in Fig. 13 as a function of C_2H_2 concentration. Both are seen to follow a similar trend, decreasing an order of magnitude when the acetylene concentration is increased a factor of four.

Similarly, decreasing the Ni film thickness from 0.5 to 0.25 μm also results in a decrease of the induction (from 2.2 to 0.7 s, respectively) and growth times (from 12 to 1.9 s, respectively, in Fig. 12b). This indicates that the bulk of the Ni film is involved in the growth process. Interestingly, very similar induction and growth times can be obtained for 0.5 μm thick films by doubling the C_2H_2 concentration from 5% to 10%.

The isothermal growth and the observed kinetics can be explained in the context of the following model, which includes

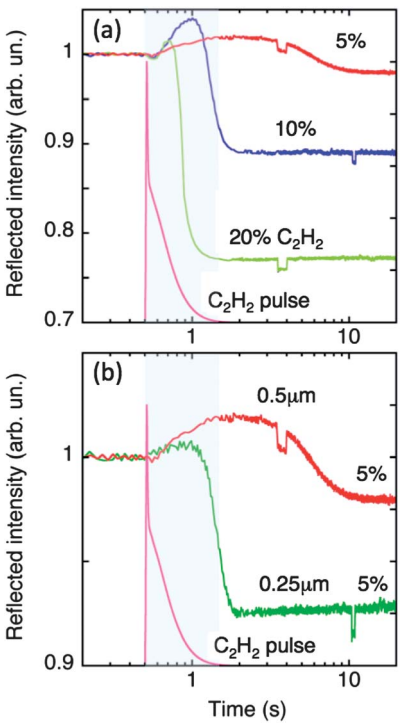

Fig. 12 Reflected intensities versus time at (a) different concentrations of C_2H_2 and (b) different Ni films thicknesses. The growth temperature in all cases was 800 °C. The calculated C_2H_2 gas pulse is shown for comparison and the vertical band marks its total duration. Note that the time scale is offset by 0.5 s to allow the use of a logarithmic scale.

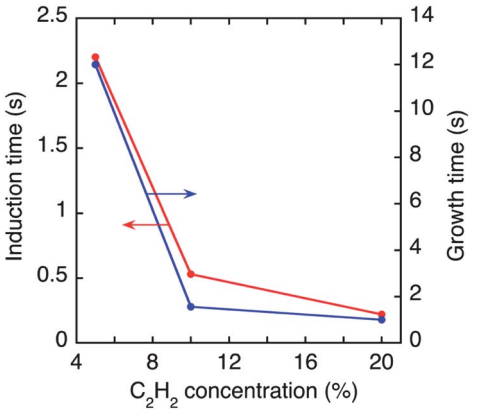

Fig. 13 Summary of the induction and growth times as a function of C_2H_2 concentration from Fig. 12a.

catalytic decomposition of C_2H_2 at the surface of the Ni film, surface nucleation of graphene, and diffusion of C atoms into the bulk of the Ni film.

In the case when the diffusion time is much shorter than the graphene nucleation time ($t_{diff} \ll t_{nucl}$) all C atoms provided by the C_2H_2 gas pulse diffuse into the Ni film. This occurs at low C_2H_2 concentrations. At the present temperatures in such thin Ni films the diffusion times are relatively short, *e.g.*, it takes only ~37 ms for carbon to diffuse the full depth of a 0.5 μm thick Ni film at 800 °C.[54] Under these conditions, and when considering the solubility of C in Ni, the maximum possible amount of carbon dissolved in Ni is only capable of supporting the growth of ~7 graphene layers.[54] Following dissolution, the second stage in graphene synthesis is the formation of graphene nuclei at the surface of the Ni film. The formation of these nuclei depletes the carbon in their vicinity and creates a concentration gradient, which drives carbon from the underlying bulk Ni to the free surface. As the graphene nuclei grow, they serve as catalysts to accelerate the flow of carbon atoms from the Ni bulk toward its surface. In this case, graphene must nucleate and grow on the Ni surface entirely from dissolved carbon. Nucleation can occur slowly, triggering accelerated growth that terminates due to carbon depletion. Such behavior can be described by typical autocatalytic kinetics.

As the C_2H_2 concentration increases, or the temperature decreases, buildup of surface/subsurface carbon can decrease the nucleation time of surface graphene to be comparable to that of the carbon diffusion time ($t_{diff} \geq t_{nucl}$). In this case, graphene nuclei begin to grow while the carbon is concentrated near the top of the film, driving faster growth from the bulk.

Even lower temperatures and higher concentrations of C_2H_2 can drive growth preferentially to the surface/subsurface mode. In this case the nucleation time is much shorter than the diffusion time ($t_{diff} \gg t_{nucl}$) and the solubility of C in Ni is also lower than in the case of higher temperatures. For example, at 675 °C the diffusion time into a 0.5 μm Ni film is ~0.45 s and decreased solubility is capable of supporting only ~4 graphene layers. In this limiting case it is possible that surface chemistry and surface growth of graphene may compete with dissolution of atomic carbon for high acetylene concentrations and lower

temperatures through the rapid formation of surface intermediates, which are difficult to dissolve.

In the context of this model, although surface processes cannot be ruled out in the pulsed-CVD experiments presented here, the observed isothermal growth and high fractional precipitation observed in this study, as well as the flux-dependence of the observed induction and growth kinetics, can be explained mainly through bulk diffusion and precipitation processes, driven by concentration gradients.

Recently, a similar kinetic growth model was described to explain the flux-dependence of the number of layers of graphene formed on Ni during isothermal growth using continuous gas introduction.[55,56] The model includes similar reaction rates for the arrival, dissolution, and precipitation of carbon. Graphene is assumed to form a monolayer on the catalyst surface when the surface carbon concentration reaches a critical value, followed by the precipitation and formation of the second layer and subsequent additional layers from carbon beneath the surface (that dissolved through leaks in the surface monolayer, see Fig. 2, ref. 56). However, our pulsed approach allows one to investigate the situation where an initial charge of carbon is injected into the Ni film and the feedstock flux is then terminated. In this case (when $t_{diff} \ll t_{nucl}$), we revealed that multiple layer graphene can precipitate quickly and isothermally from dissolved carbon after an induction time, at a time after the surface concentration of carbon exceeds its maximum, which is contrary to this model. As revealed in the imaging and reflectivity studies above, in this case graphene is observed to nucleate in multiple patches after an induction time that can exceed the duration of the gas pulse. In this case nucleation and growth appear to follow autocatalytic kinetics with induction times for surface graphene nucleation determined by subsurface carbon concentration levels. Detailed kinetics will be published elsewhere.

Conclusions

The kinetics and mechanisms of graphene growth on Ni films were studied using a pulsed CVD approach combined with real-time optical diagnostics. *In situ* UV-Raman spectroscopy with simultaneous detection of both the G- and 2D-bands was used to unambiguously detect isothermal graphene growth at high temperatures, measure the growth kinetics with ~1 s temporal resolution, and estimate the fractional precipitation upon cooldown. Optical reflectivity and videography provided much faster temporal resolution. Both the growth kinetics and the fractional isothermal precipitation were found to be governed by the C_2H_2 partial pressure in the CVD pulse for a given film thickness and temperature. Graphene precipitation during cooling was shown to occur above 600 °C. Room-temperature Raman spectroscopy and mapping of as-grown and transferred graphene grown by single, sub-second acetylene pulses at low partial pressures and high temperatures showed turbostratic bilayer graphene with low defect density intermixed with few-layer graphene patches.

Higher acetylene partial pressures were found to drive larger fractions of isothermal graphene growth and shorter nucleation and growth periods. For example, at 800 °C up to 94% of graphene growth occurs isothermally within the ~1 second acetylene gas lifetime in the growth chamber. The possible role of autocatalytic surface chemical reactions should be considered as a growth mechanism (along with dissolution/precipitation) since very similar flux-dependent nucleation and growth kinetics were observed in similar experiments in the pulsed-CVD growth of SWNTs.[24,25]

However, at lower acetylene partial pressures the bulk of the Ni film was clearly involved in the growth. Isothermal graphene growth was observed ~10 seconds *after* the growth gas was cleared from the chamber, and this growth time was shown to significantly shorten when the thickness of the Ni film was reduced. These results were explained in the context of a dissolution/precipitation model incorporating a flux-dependent induction time to form graphene nuclei, and subsequent deposition from dissolved carbon driven by concentration gradients.

Time-resolved reflectivity and microscope-based videography of graphene growth kinetics were shown to agree with those obtained from Raman experiments, indicating that these easily-implementable techniques can be used as fast diagnostics of graphene growth at high temperatures. Since the nucleation time, growth rate, and product distribution can be expected to vary with the partial pressure of acetylene in the pulse (as shown for SWNTs)[24,25] pulsed CVD coupled with fast, *in situ* optical diagnostics opens new possibilities to explore and control the flux-dependent growth kinetics and mechanisms of this process for rapid synthesis and processing of graphene with controlled number of layers.

Acknowledgements

Synthesis science sponsored by the Materials Sciences and Engineering (MSE) Division, Office of Basic Energy Sciences, U.S. Department of Energy. Characterization science including Raman spectroscopy and SEM part of this research was conducted at the Center for Nanophase Materials Sciences user facility, which is sponsored at Oak Ridge National Laboratory by the Scientific User Facilities (SUF) Division, U.S. Department of Energy.

Notes and references

1 K. S. Novoselov, Nobel Lecture: Graphene: Materials in the Flatland, *Rev. Mod. Phys.*, 2011, **83**, 837–849.
2 M. H. Rummeli, C. G. Rocha, F. Ortmann, I. Ibrahim, H. Sevincli, F. Borrnert, J. Kunstmann, A. Bachmatiuk, M. Potschke, M. Shiraishi, M. Meyyappan, B. Buchner, S. Roche and G. Cuniberti, Graphene: Piecing it Together, *Adv. Mater.*, 2011, **23**, 4471–4490.
3 N. S. Safron, M. Kim, P. Gopalan and M. S. Arnold, Barrier-Guided Growth of Micro- and Nano-Structured Graphene, *Adv. Mater.*, 2012, **24**, 1041–1045.
4 X. S. Li, W. W. Cai, J. H. An, S. Kim, J. Nah, D. X. Yang, R. Piner, A. Velamakanni, I. Jung, E. Tutuc, S. K. Banerjee, L. Colombo and R. S. Ruoff, Large-Area Synthesis of High-Quality and

Uniform Graphene Films on Copper Foils, *Science*, 2009, **324**, 1312–1314.
5 X. S. Li, C. W. Magnuson, A. Venugopal, R. M. Tromp, J. B. Hannon, E. M. Vogel, L. Colombo and R. S. Ruoff, Large-Area Graphene Single Crystals Grown by Low-Pressure Chemical Vapor Deposition of Methane on Copper, *J. Am. Chem. Soc.*, 2011, **133**, 2816–2819.
6 S. Lee, K. Lee and Z. H. Zhong, Wafer Scale Homogeneous Bilayer Graphene Films by Chemical Vapor Deposition, *Nano Lett.*, 2010, **10**, 4702–4707.
7 Z. T. Luo, Y. Lu, D. W. Singer, M. E. Berck, L. A. Somers, B. R. Goldsmith and A. T. C. Johnson, Effect of Substrate Roughness and Feedstock Concentration on Growth of Wafer-Scale Graphene at Atmospheric Pressure, *Chem. Mater.*, 2011, **23**, 1441–1447.
8 I. Vlassiouk, M. Regmi, P. F. Fulvio, S. Dai, P. Datskos, G. Eres and S. Smirnov, Role of Hydrogen in Chemical Vapor Deposition Growth of Large Single-Crystal Graphene, *ACS Nano*, 2011, **5**, 6069–6076.
9 M. Regmi, M. F. Chisholm and G. Eres, The Effect of Growth Parameters on the Intrinsic Properties of Large-Area Single Layer Graphene Grown by Chemical Vapor Deposition on Cu, *Carbon*, 2012, **50**, 134–141.
10 L. Tao, J. Lee, H. Chou, M. Holt, R. S. Ruoff and D. Akinwande, Synthesis of High Quality Monolayer Graphene at Reduced Temperature on Hydrogen-Enriched Evaporated Copper (111) Films, *ACS Nano*, 2012, **6**, 2319–2325.
11 J. D. Wood, S. W. Schmucker, A. S. Lyons, E. Pop and J. W. Lyding, Effects of Polycrystalline Cu Substrate on Graphene Growth by Chemical Vapor Deposition, *Nano Lett.*, 2011, **11**, 4547–4554.
12 C. Mattevi, H. Kim and M. Chhowalla, A Review of Chemical Vapour Deposition of Graphene on Copper, *J. Mater. Chem.*, 2011, **21**, 3324–3334.
13 Q. K. Yu, J. Lian, S. Siriponglert, H. Li, Y. P. Chen and S. S. Pei, Graphene Segregated on Ni Surfaces and Transferred to Insulators, *Appl. Phys. Lett.*, 2008, **93**, 113103.
14 K. S. Kim, Y. Zhao, H. Jang, S. Y. Lee, J. M. Kim, K. S. Kim, J. H. Ahn, P. Kim, J. Y. Choi and B. H. Hong, Large-Scale Pattern Growth of Graphene Films for Stretchable Transparent Electrodes, *Nature*, 2009, **457**, 706–710.
15 S. J. Chae, F. Gunes, K. K. Kim, E. S. Kim, G. H. Han, S. M. Kim, H. J. Shin, S. M. Yoon, J. Y. Choi, M. H. Park, C. W. Yang, D. Pribat and Y. H. Lee, Synthesis of Large-Area Graphene Layers on Poly-Nickel Substrate by Chemical Vapor Deposition: Wrinkle Formation, *Adv. Mater.*, 2009, **21**, 2328–2333.
16 A. Reina, X. T. Jia, J. Ho, D. Nezich, H. B. Son, V. Bulovic, M. S. Dresselhaus and J. Kong, Large Area, Few-Layer Graphene Films on Arbitrary Substrates by Chemical Vapor Deposition, *Nano Lett.*, 2009, **9**, 30–35.
17 A. Reina, S. Thiele, X. T. Jia, S. Bhaviripudi, M. S. Dresselhaus, J. A. Schaefer and J. Kong, Growth of Large-Area Single- and Bi-Layer Graphene by Controlled Carbon Precipitation on Polycrystalline Ni Surfaces, *Nano Res.*, 2009, **2**, 509–516.
18 H. J. Park, J. Meyer, S. Roth and V. Skakalova, Growth and Properties of Few-Layer Graphene Prepared by Chemical Vapor Deposition, *Carbon*, 2010, **48**, 1088–1094.
19 Y. Zhang, L. Gomez, F. N. Ishikawa, A. Madaria, K. Ryu, C. A. Wang, A. Badmaev and C. W. Zhou, Comparison of Graphene Growth on Single-Crystalline and Polycrystalline Ni by Chemical Vapor Deposition, *J. Phys. Chem. Lett.*, 2010, **1**, 3101–3107.
20 Z. Y. Juang, C. Y. Wu, A. Y. Lu, C. Y. Su, K. C. Leou, F. R. Chen and C. H. Tsai, Graphene Synthesis by Chemical Vapor Deposition and Transfer by a Roll-to-Roll Process, *Carbon*, 2010, **48**, 3169–3174.
21 X. Liu, L. Fu, N. Liu, T. Gao, Y. F. Zhang, L. Liao and Z. F. Liu, Segregation Growth of Graphene on Cu–Ni Alloy for Precise Layer Control, *J. Phys. Chem. C*, 2011, **115**, 11976–11982.
22 J. M. Wofford, S. Nie, K. F. McCarty, N. C. Bartelt and O. D. Dubon, Graphene Islands on Cu Foils: The Interplay between Shape, Orientation, and Defects, *Nano Lett.*, 2010, **10**, 4890–4896.
23 X. S. Li, W. W. Cai, L. Colombo and R. S. Ruoff, Evolution of Graphene Growth on Ni and Cu by Carbon Isotope Labeling, *Nano Lett.*, 2009, **9**, 4268–4272.
24 A. A. Puretzky, D. B. Geohegan, J. J. Jackson, S. Pannala, G. Eres, C. M. Rouleau, K. L. More, N. Thonnard and J. D. Readle, Incremental Growth of Short SWNT Arrays by Pulsed Chemical Vapor Deposition, *Small*, 2012, **8**, 1534–1542.
25 D. B. Geohegan, A. A. Puretzky, J. J. Jackson, C. M. Rouleau, G. Eres and K. L. More, Flux-Dependent Growth Kinetics and Diameter Selectivity in Single-Wall Carbon Nanotube Arrays, *ACS Nano*, 2011, **5**, 8311–8321.
26 J. J. Jackson, A. A. Puretzky, K. L. More, C. M. Rouleau, G. Eres and D. B. Geohegan, Pulsed Growth of Vertically Aligned Nanotube Arrays with Variable Density, *ACS Nano*, 2010, **4**, 7573–7581.
27 J. B. Park, W. Xiong, Y. Gao, M. Qian, Z. Q. Xie, M. Mitchell, Y. S. Zhou, G. H. Han, L. Jiang and Y. F. Lu, Fast Growth of Graphene Patterns by Laser Direct Writing, *Appl. Phys. Lett.*, 2011, **98**, 123109.
28 K. L. Saenger, J. C. Tsang, A. A. Bol, J. O. Chu, A. Grill and C. Lavoie, *In Situ* X-ray Diffraction Study of Graphitic Carbon Formed During Heating and Cooling of Amorphous-C/Ni Bilayers, *Appl. Phys. Lett.*, 2010, **96**, 153105.
29 A. Gruneis, K. Kummer and D. V. Vyalikh, Dynamics of Graphene Growth on a Metal Surface: A Time-Dependent Photoemission Study, *New. J. Phys.*, 2009, **11**, 073050.
30 R. S. Weatherup, B. C. Bayer, R. Blume, C. Ducati, C. Baehtz, R. Schlogl and S. Hofmann, *In Situ* Characterization of Alloy Catalysts for Low-Temperature Graphene Growth, *Nano Lett.*, 2011, **11**, 4154–4160.
31 M. Losurdo, M. M. Giangregorio, P. Capezzuto and G. Bruno, Ellipsometry as a Real-Time Optical Tool for Monitoring and Understanding Graphene Growth on Metals, *J. Phys. Chem. C*, 2011, **115**, 21804–21812.
32 A. A. Puretzky, D. B. Geohegan, S. Jesse, I. N. Ivanov and G. Eres, *In Situ* Measurements and Modeling of Carbon Nanotube Array Growth Kinetics During Chemical Vapor

Deposition, *Appl. Phys. A: Mater. Sci. Process.*, 2005, **81**, 223–240.
33 N. Latorre, E. Romeo, F. Cazana, T. Ubieto, C. Royo, J. J. Villacampa and A. Monzon, Carbon Nanotube Growth by Catalytic Chemical Vapor Deposition: A Phenomenological Kinetic Model, *J. Phys. Chem. C*, 2010, **114**, 4773–4782.
34 G. Eres, C. M. Rouleau, M. Yoon, A. A. Puretzky, J. J. Jackson and D. B. Geohegan, Model for Self-Assembly of Carbon Nanotubes from Acetylene Based on Real-Time Studies of Vertically Aligned Growth Kinetics, *J. Phys. Chem. C*, 2009, **113**, 15484–15491.
35 A. Magrez, R. Smajda, J. W. Seo, E. Horvath, P. R. Ribic, J. C. Andresen, D. Acquaviva, A. Olariu, G. Laurenczy and L. Forro, Striking Influence of the Catalyst Support and Its Acid–Base Properties: New Insight into the Growth Mechanism of Carbon Nanotubes, *ACS Nano*, 2011, **5**, 3428–3437.
36 F. Ding, A. R. Harutyunyan and B. I. Yakobson, Dislocation Theory of Chirality-Controlled Nanotube Growth, *Proc. Natl. Acad. Sci. U. S. A.*, 2009, **106**, 2506–2509.
37 E. Loginova, N. C. Bartelt, P. J. Feibelman and K. F. McCarty, Evidence for Graphene Growth by C Cluster Attachment, *New J. Phys.*, 2008, **10**, 093026.
38 M. Balkanski, R. F. Wallis and E. Haro, Anharmonic Effects in Light-Scattering Due to Optical Phonons in Silicon, *Phys. Rev. B: Condens. Matter Mater. Phys.*, 1983, **28**, 1928–1934.
39 E. Haro, M. Balkanski, R. F. Wallis and K. H. Wanser, Theory of the Anharmonic Damping and Shift of the Raman Mode in Silicon, *Phys. Rev. B: Condens. Matter Mater. Phys.*, 1986, **34**, 5358–5367.
40 A. Tiberj, N. Camara, P. Godignon and J. Camassel, Micro-Raman and micro-transmission imaging of epitaxial graphene grown on the Si and C faces of 6H-SiC, *Nanoscale Res. Lett.*, 2011, **6**, 478.
41 E. N. Voloshina and Y. S. Dedkov, Graphene on metallic surfaces: problems and perspectives, *Phys. Chem. Chem. Phys.*, 2012, **14**, 13502–13514.
42 K. Takahashi, K. Yamada, H. Kato, H. Hibino and Y. Homma, *In situ* scanning electron microscopy of graphene growth on polycrystalline Ni substrate, *Surf. Sci.*, 2012, **606**, 728–732.
43 Z. Ni, Y. Wang, T. Yu, Y. You and Z. Shen, Reduction of Fermi velocity in folded graphene observed by resonance Raman spectroscopy, *Phys. Rev. B: Condens. Matter Mater. Phys.*, 2008, **77**, 235403.
44 W. Fang, A. L. Hsu, R. Caudillo, Y. Song, A. G. Birdwell, E. Zakar, M. Kalbac, M. Dubey, T. Palacios, M. S. Dresselhaus, P. T. Araujo and J. Kong, Rapid Identification of Stacking Orientation in Isotopically Labeled Chemical-Vapor Grown Bilayer Graphene by Raman Spectroscopy, *Nano Lett.*, 2013, **13**, 1541–1548.
45 I. Calizo, I. Bejenari, M. Rahman, G. Liu and A. A. Balandin, Ultraviolet Raman Microscopy of Single and Multilayer Graphene, *J. Appl. Phys.*, 2009, **106**, 043509.
46 N. Bonini, R. Rao, A. M. Rao, N. Marzari and J. Menendez, Lattice Anharmonicity in Low-dimensional Carbon Systems, *Phys. Status Solidi B*, 2008, **245**, 2149–2154.
47 K. T. Nguyen, D. Abdula, C. L. Tsai and M. Shim, Temperature and Gate Voltage Dependent Raman Spectra of Single-Layer Graphene, *ACS Nano*, 2011, **5**, 5273–5279.
48 A. Li-Pook-Than, J. Lefebvre and P. Finnie, Phases of Carbon Nanotube Growth and Population Evolution from *In Situ* Raman Spectroscopy During Chemical Vapor Deposition, *J. Phys. Chem. C*, 2010, **114**, 11018–11025.
49 S. Chiashi, Y. Murakami, Y. Miyauchi and S. Maruyama, Cold wall CVD generation of single-walled carbon nanotubes and *in situ* Raman scattering measurements of the growth stage, *Chem. Phys. Lett.*, 2004, **386**, 89–94.
50 K. Kaminska, J. Lefebvre, D. G. Austing and P. Finnie, Real-time *in situ* Raman imaging of carbon nanotube growth, *Nanotechnology*, 2007, **18**(16), 165707.
51 M. Picher, E. Anglaret, R. Arenal and V. Jourdain, Self-Deactivation of Single-Walled Carbon Nanotube Growth Studied by *In Situ* Raman Measurements, *Nano Lett.*, 2009, **9**, 542–547.
52 P. Finnie, A. Li-Pook-Than and J. Lefebvre, The Dynamics of the Nucleation, Growth and Termination of Single-Walled Carbon Nanotubes from *In situ* Raman Spectroscopy During Chemical Vapor Deposition, *Nano Res.*, 2009, **2**, 783–792.
53 R. Rao, D. Liptak, T. Cherukuri, B. I. Yakobson and B. Maruyama, *In situ* evidence for chirality-dependent growth rates of individual carbon nanotubes, *Nat. Mater.*, 2012, **11**, 213–216.
54 L. Baraton, Z. B. He, C. S. Lee, C. S. Cojocaru, M. Chatelet, J.-L. Maurice, Y. H. Lee and D. Pribat, On the mechanisms of precipitation of graphene on nickel thin films, *EPL*, 2011, **96**, 46003.
55 R. S. Weatherup, B. C. Bayer, R. Blume, C. Baehtz, P. R. Kidambi, M. Fouquet, C. T. Wirth, R. Schlogl and S. Hofmann, On the Mechanisms of Ni-Catalysed Graphene Chemical Vapour Deposition, *ChemPhysChem*, 2012, **13**, 2544–2549.
56 R. S. Weatherup, B. Dlubak and S. Hofmann, Kinetic Control of Catalytic CVD for High-Quality Graphene at Low Temperatures, *ACS Nano*, 2012, **6**, 9996–10003.